Supplementary information for

Experimental Demonstration of Feature Extraction and Dimensionality Reduction using Memristor Networks

Shinhyun Choi, † Jong Hoon Shin, † Jihang Lee, Patrick Sheridan, and Wei D. Lu*

Department of Electrical Engineering and Computer Science, the University of Michigan, Ann Arbor, Michigan 48109, USA

1. Device Modeling

The numerical simulations are based on a memristor model developed in ref [S1]. The internal state variable, w, represents the effective area covered by the conductive channel. The current through the device is described by Eq. S1, consisting of conduction through the channel area (first term) and the rest of the device (second term). The dynamics of the state variable under the applied voltage is shown in Eq. S2. Here γ, δ, α, β are positive parameters related to material properties such as the effective tunneling distance, tunneling barrier, the depletion width

of the Schottky barrier region and Schottky barrier height, $u(\ )$ is the Heaviside step function, k, μ_1, u_2, are positive parameters determined by material properties such as ion hopping distance and hopping barrier heights [S1].

$$I = w\,\gamma \sinh(\delta \times V) + (1-w)\alpha\left(1 - e^{-\beta \times V)}\right) \quad \text{(S1)}$$

$$\frac{dw}{dt} = (w-1)^2 k(e^{-\mu_1 V} - e^{\mu_2 V})u(-V) + w^2 k(e^{-\mu_1 V} - e^{\mu_2 V})u(V) \quad \text{(S2)}$$

The memristor model, consisting of the *I-V* equation (S1) and the state variable dynamic equation (S2), shows good agreements with experimental results, as shown in Fig. 1(d).

2. PCA implementation in memristor networks

As discussed in the main text, the output vector is determined by the dot-product of the input vector and the memristor weight matrix, while the network learns the principal components by adjusting the weights of the memristor network during training. To map the physical parameters obtained in the memristor network with the parameters used in PCA analysis and Sanger's rule, a linear transformation is needed.

To obtain an output value y_j from the jth column, a vector of 9 input voltage pulses with fixed amplitude (V_0 = 0.3 V) and variable pulse widths (0 to 1000 μs duration with 100 μs unit pulse width) proportional to the value of the input data x_i (dimensionless integer from 1 to 10) is applied to the 9 rows. The amount of charge Q_j collected at the j^{th} column in the memristor network is then obtained

$$Q_j = \sum_i I_{ij}\, t_i = \sum_i I_{ij}\, t_0 x_i \quad \text{(S3)}$$

where I_{ij} is the current through the device at i^{th} row and j^{th} column, t_i is the duration of the input pulse, and t_0=100 μs is the unit pulse width. From the current expression in Eq. (S1), Eq. (S3) can be re-written as

$$Q_j = \sum_i \left[w_{ij} \gamma \sinh(\delta \times V_0) + \left(1 - w_{ij}\right) \alpha \left(1 - e^{-\beta \times V_0)}\right) \right] t_0 x_i \quad \text{(S4)}$$

$$= \sum_i \left[w_{ij} A + \left(1 - w_{ij}\right) B \right] x_i \quad \text{(S5)}$$

where

$$A = \gamma \sinh(\delta \times V_0) \times t_0 \,, \; B = \alpha \left(1 - e^{-\beta \times V_0)}\right) \times t_0 \quad \text{(S6)}$$

are constants depending on the device parameters γ, δ, α, and β, and experimental parameters V_0 and t_0. A and B have units of charge.

The output y used to perform the PCA analysis is then obtained from the charge Q_j inEq. S4 as following:

$$y_j = \frac{2Q_j}{A-B} - \sum_i \left[\frac{A+B}{A-B} x_i \right] = \sum_{i=1}^{n} g_{ij} x_i \quad \text{(S7)}$$

where

$$g_{ij} = 2w_{ij} - 1 \quad \text{(S8)}$$

Here g, x, and y are all dimensionless values. Eq. (S7) shows that the output y_j at neuron j is determined by the dot-product of the input vector x and the weight vector g_j. Furthermore, y and g_{ij} obtained in Eqs. S7 and S8 are used to perform the weight updates and PCA analysis

following Sanger's rule (Eq. 1 in the main text). After training, the weights g_{ij} in columns 1 and 2 form the (first and 2nd, respectively) principal components of the input data set.

3. Training time calculation

From the Sanger's rule shown in Eq. (1), the desired weight update Δg_{ij} can be calculated. Programming voltage pulses are then applied to the inputs to modify the memristor weights. The training pulses are determined by the polarity and magnitude of Δg_{ij}, with potentiation (1.1 V) pulses for positive Δg_{ij} and depression (-1.4 V) pulses for negative Δg_{ij}, while the pulse widths are determined by the magnitude of $\left|\Delta g_{ij}\right|$ and g_{ij}. Here, from Eq. S2, a simple approach is used to compensate for the non-linear response of the internal state variable *w*. Specifically, the pulse width $\left|\Delta \mathrm{t}\right|$ is determined as

$$\Delta t_{ij} = \frac{2}{k\left(e^{-\mu_1 V_{potentiation}} - e^{\mu_2 V_{potentiation}}\right)}\left(\frac{-1}{g_{ij}+\Delta g_{ij}-1} + \frac{1}{g_{ij}-1}\right) u(\Delta \mathrm{g})$$

$$+ \frac{2}{k\left(e^{-\mu_1 V_{depression}} - e^{\mu_2 V_{depression}}\right)}\left(\frac{-1}{g_{ij}+\Delta g_{ij}+1} + \frac{1}{g_{ij}+1}\right) u(-\Delta \mathrm{g}). \quad \text{(S9)}$$

where *u*( ) is the Heaviside step function. The parameters used in the model are listed in Table S1

Equations	Parameters	Values
I-V Equation (Eq.S1)	α	1.58×10^{-3}
	β	0.5
	γ	3.01×10^{-3}
	δ	0.5
State variable dynamic equation (Eq.S2)	k	1.0×10^{-4}
	μ_1	19.25
	μ_2	13
Sanger's rule (Eq.1)	η	0.001

Table S1. List of parameters used in the model.

4. Annealing treatment to create forming-free devices

Fabrication of forming-free devices is essential for the reliable operation of an memristor array, since non-selected (particularly half-selected) devices in the passive crossbar can be severely damaged if high-voltage forming processes are required. To eliminate high-voltage forming, we utilized rapid thermal processing (RTP) during device fabrication to create the desired oxygen vacancy profile. During the RTP process, oxygen atoms in the Ta_2O_5 layer react with the Ta top electrode (TE) and create oxygen vacancies at the Ta TE/Ta_2O_5 interface. The induced oxygen vacancies will further diffuse from the interface into the Ta_2O_5 layer and create the desired oxygen vacancy profile for resistive switching. [S3-4] This process has been shown to reduce the forming voltage and make the devices essentially forming-free. Figure S1a shows the I-V characteristics of virgin devices after device annealing at different annealing times. As the annealing time increases, the current level increases and the forming voltage decreases. After

15 min annealing, reliable switching can be obtained in the device without any forming process, as shown in Fig. S1b.

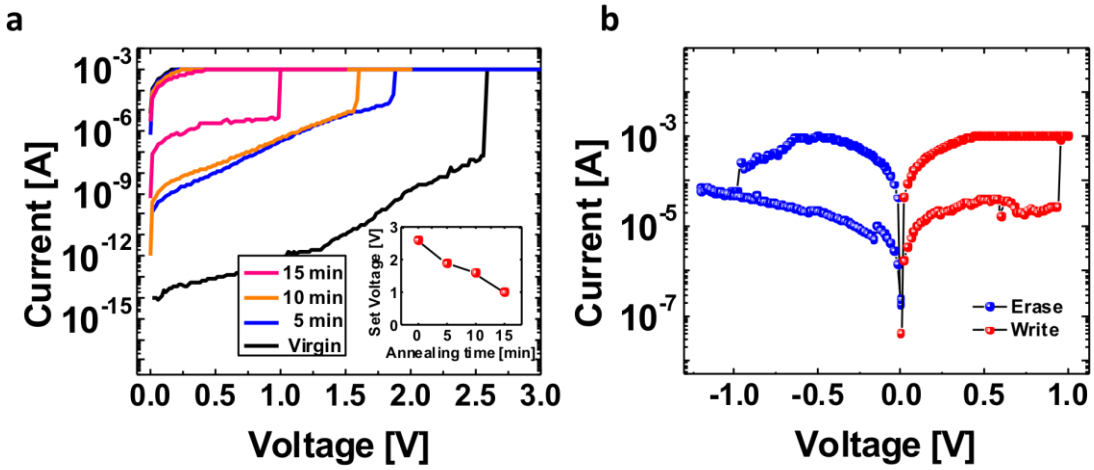

Figure S1. Forming-free devices created through annealing. (a) I-V characteristics as a function of total annealing time. (b) Switching characteristics of a virgin device after annealing.

5. Circuit schematic of the test board

A schematic of the test board is shown in Fig. S2. There are 4 digital-to-analog converters (DACs) on the test board to supply voltage pulses ranging from 0V to 5.0V on the selected bottom electrode (through DAC1), the unselected bottom electrodes (through DAC2), the selected top electrode (through DAC3), and the unselected top electrodes (through DAC4), respectively. Matrix switches (Switch1, Switch2) allocate each memristive device to the corresponding DAC. To measure current through a memristive device in the array, a multiplexer (MUX) is activated so as to flow the current into an analog-to-digital converter (ADC), while the

unselected rows and the unselected column are grounded to prevent sneak path current during the read process. Due to the virtual ground of the op-amp, the voltage biased on a sensing resistor (1kΩ) is measured using ADC and converted to the current value. The arrows in the schematic Fig. S2 indicate the current path through a selected memristive device for write, erase, and read processes. The bias voltage of each DAC for each process is specified in the legend of Fig. S2.

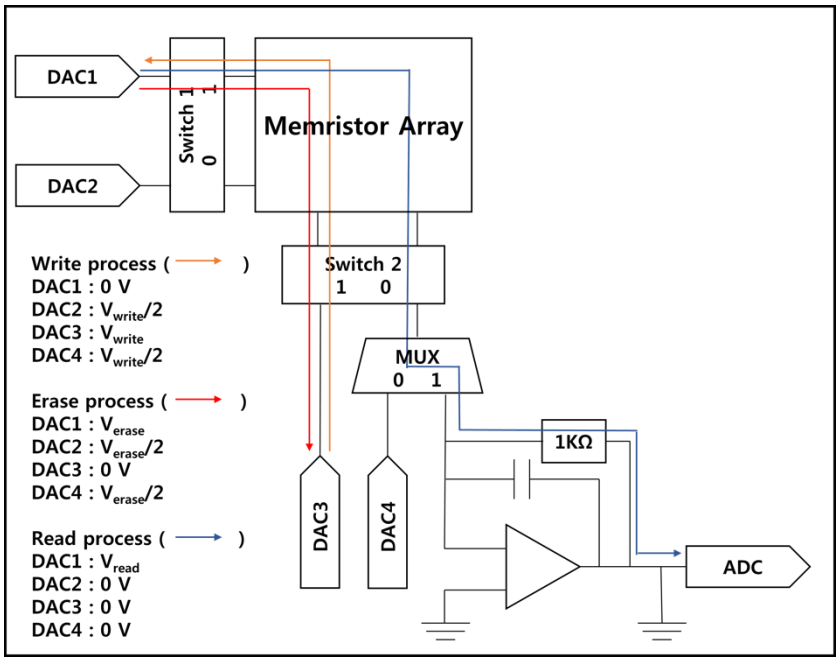

Figure S2. Circuit schematic of the test board.

6. Test board operation

Fig. S3 shows the flow chart of the test board to implement PCA analysis. The initial output is obtained with V_{READ}. With randomly sequenced training sets, the desired weight changes and applied pulse widths are calculated following Sanger's rule as discussed in Sections 2-3. After adjusting the memristor weights, the updated outputs are obtained using another read

process. This procedure is then repeated for the 100 training data points, over the desired training cycles (35 cycles).

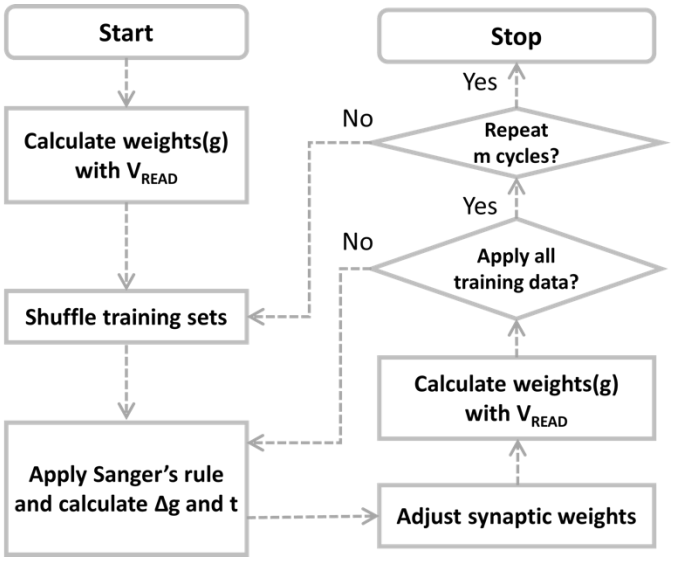

Figure S3. Flow chart of the PCA network operation.

7. Details of weight distributions

Weight distributions for the primary and the secondary principal components after each training cycle are plotted in Figs. S4a and S4b, respectively. For the primary principal component, the weights update is completed quickly and the weights in general become stabilized after only a few training cycles. While for the secondary principal component, the weights normally need longer time to be stabilized. The reason behind the difference is that the successful training of the secondary principal component using Sanger's rule depends on the stabilization of the primary principal component, and the secondary principal component starts to be stabilized only after all the weights in the primary principal component become stabilized.

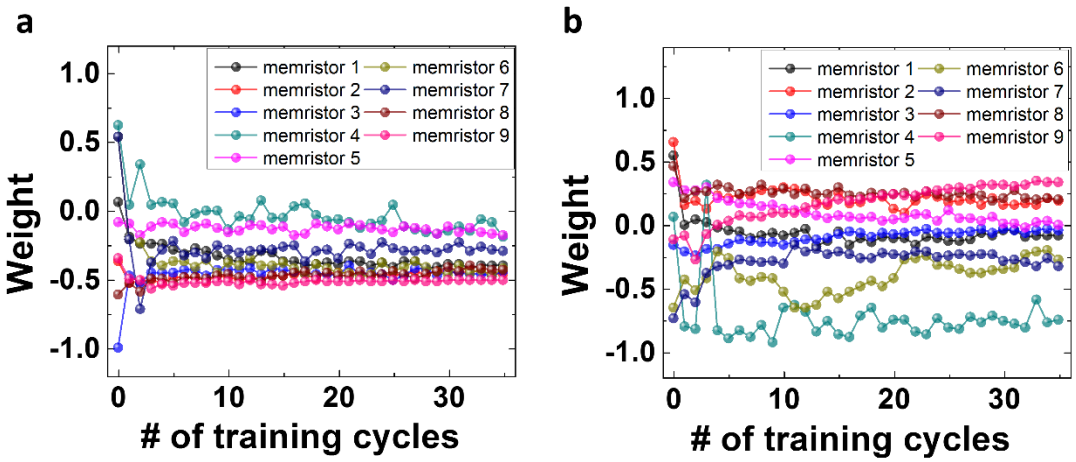

Figure S4. Weight updates as a function of training cycles, for (a) the primary principal component, and (b) the secondary principal component.

8. Device variations

Figure S5 shows the analog conductance changes of the 18 memristor devices forming the network. Device-device variations are observed both at the initial state and after potentiation/depression pulses. The devices were subjected to 50 potentiation pulses (1.1 V, 3 μs) followed by 50 depression pulses (-1.4 V, 30 μs), and the conductance was measured with 0.3V, 1 ms read pulses after each potentiation or depression pulse. The network can tolerate the device variations during unsupervised learning and settle down to the desired principal components and produce correct classification results.

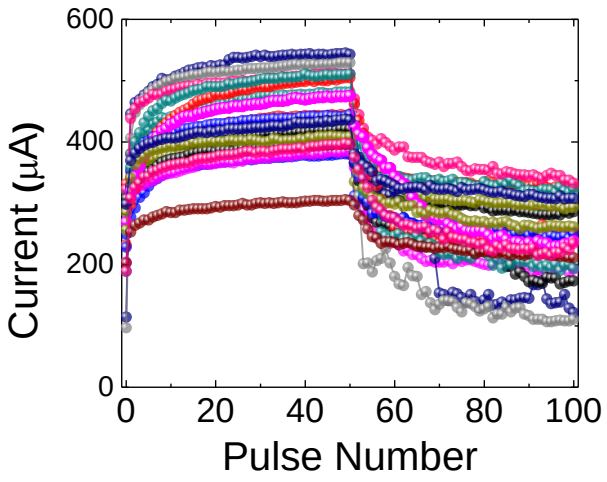

Figure S5. Conductances measured from all 18 memristor devices in the network, showing device-to-device variations and analog conductance changes.

9. PCA analysis by directly solving the covariance matrix

In classical PCA analysis, the features of a dataset can be extracted by directly solving the eigenvalue problem of the covariance matrix. Using the PCA module in Python codes, an exact solution was obtained and used for the feature extraction of the breast cancer data to compare with the results obtained from the memristor network (Fig. 2 in the main text). After clustering of the data, a decision boundary for prediction of breast cancer was calculated by fitting the training data set with the logistic regression algorithm (Figure S6a). In Fig.S6b, the test data set was used to validate the classification result and an accuracy of 97.6% based on the exact PCA solutions obtained in software.

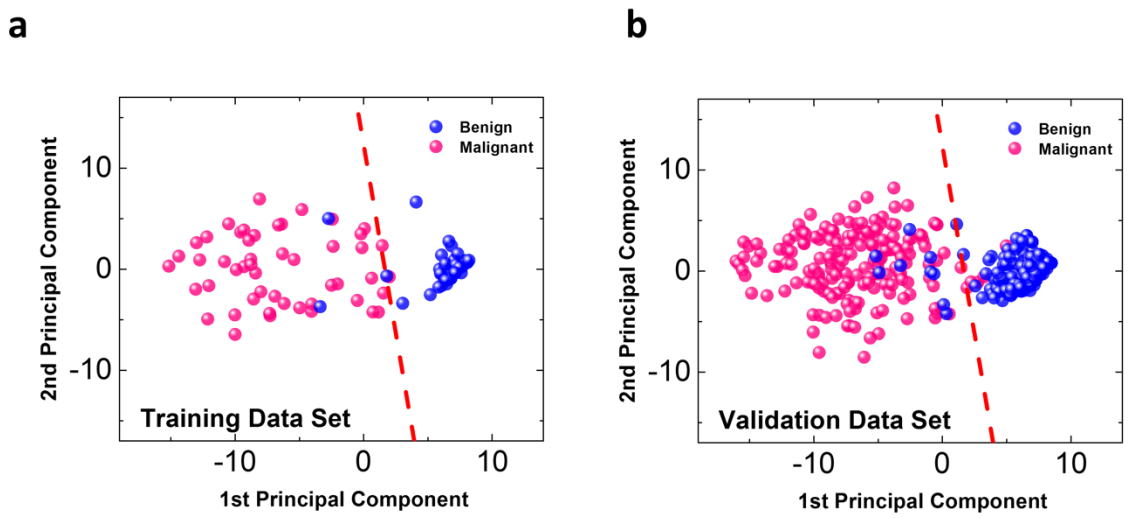

Figure S6. Classification results based on the exact solution of PCA. (a) Decision boundary (dotted line) obtained by fitting the training data set using logistic regression. (b) The decision boundary calculated from (a) overlaid with test data after PCA analysis. Prediction was made based on a data point's location with respect to the decision boundary. The blue and magenta color labels represent the ground truth.

The views expressed in this paper are those of the authors and do not reflect the official policy or position of the Department of Defense or the U.S. Government. Approved for Public Release. Distribution unlimited.

REFERENCES

(S1) Chang, T., Jo, S., Kim, K.H., Sheridan, P., Gaba, S. & Lu, W. Synaptic behaviors and modeling of a metal oxide memristive device. *Appl. Phys. A*, **102**, 857-63 (2011).

(S2) Choi, S., Sheridan, P., & Lu, W. D. Data clustering using memristor networks. Sci. Rep. **5**, 10492 (2015).

(S3) Sung, M. G., Kim, S. J., Joo, M. S., Roh, J. S., Ryu, C., Hong, S., Kim, H. & Kim, Y. S. Effect of the oxygen vacancy gradient in titanium dioxide on the switching direction of bipolar resistive memory. Solid-State Electron., **63**, 115-118 (2011).

(S4) Kim, S., Choi, S. H., Lu, W. Comprehensive physical model of dynamic resistive switching in an oxide memristor. ACS Nano, **8**, 2369-2376.(2014).